gene expression (to 1.3 ± 0.3-fold, $P < 0.05$ and 1.0 ± 0.3 fold, $P < 0.05$), when compared with Ang II-alone mice (2.6 ± 1.0 fold, 3.2 ± 2.0-fold, respectively). Parallel to the change in collagen gene expression, tenascin-C mRNA levels in Ang II-treated and aldosterone-treated groups were significantly upregulated (11.2 ± 5.8-fold increase for Ang II, $P < 0.05$ and 2.6 ± 0.6-fold for aldosterone, $P < 0.001$) compared with the control mice (1.0 ± 0.2). Eplerenone treatment significantly abrogated the induction of tenascin-C expression by Ang II (2.3 ± 1.3-fold, $P < 0.05$).

Macrophage Infiltration

Immunohistologic analysis demonstrated many Mac 3 positive macrophages to have accumulated in the perivascular spaces in Ang II-treated mice, whereas only a few macrophages were observed in control mice (14.3 ± 3.4 vs 1.8 ± 0.9 cells/optic field, $P < 0.05$; Fig. 3A). In Ang II/eplerenone-treated mice, the number of macrophages was significantly reduced (4.5 ± 2.9 cells/optic field, $P < 0.05$) as compared with the Ang II-alone case. Aldosterone treatment also caused an increase of the number of macrophages (6.7 ± 1.25 cells/optic field, $P < 0.01$).

Expression of Cytokines and Growth Factors

Immunostaining demonstrated that Ang II treatment significantly increased the numbers of PDGF-A–(Fig. 3B) and PDGF-B–(Fig. 3C) positive cells in the perivascular region as compared with the controls (17.83 ± 3.37 vs 7.11 ± 1.67 cells/optic field, $P < 0.01$, 32.3 ± 7.2 vs 8.23 ± 3.35 cells/optic field, $P < 0.001$, respectively). Aldosterone treatment also significantly increased the number of PDGF-A and -B positive cells (12.72 ± 0.97 vs 7.11 ± 1.67 cells/optic

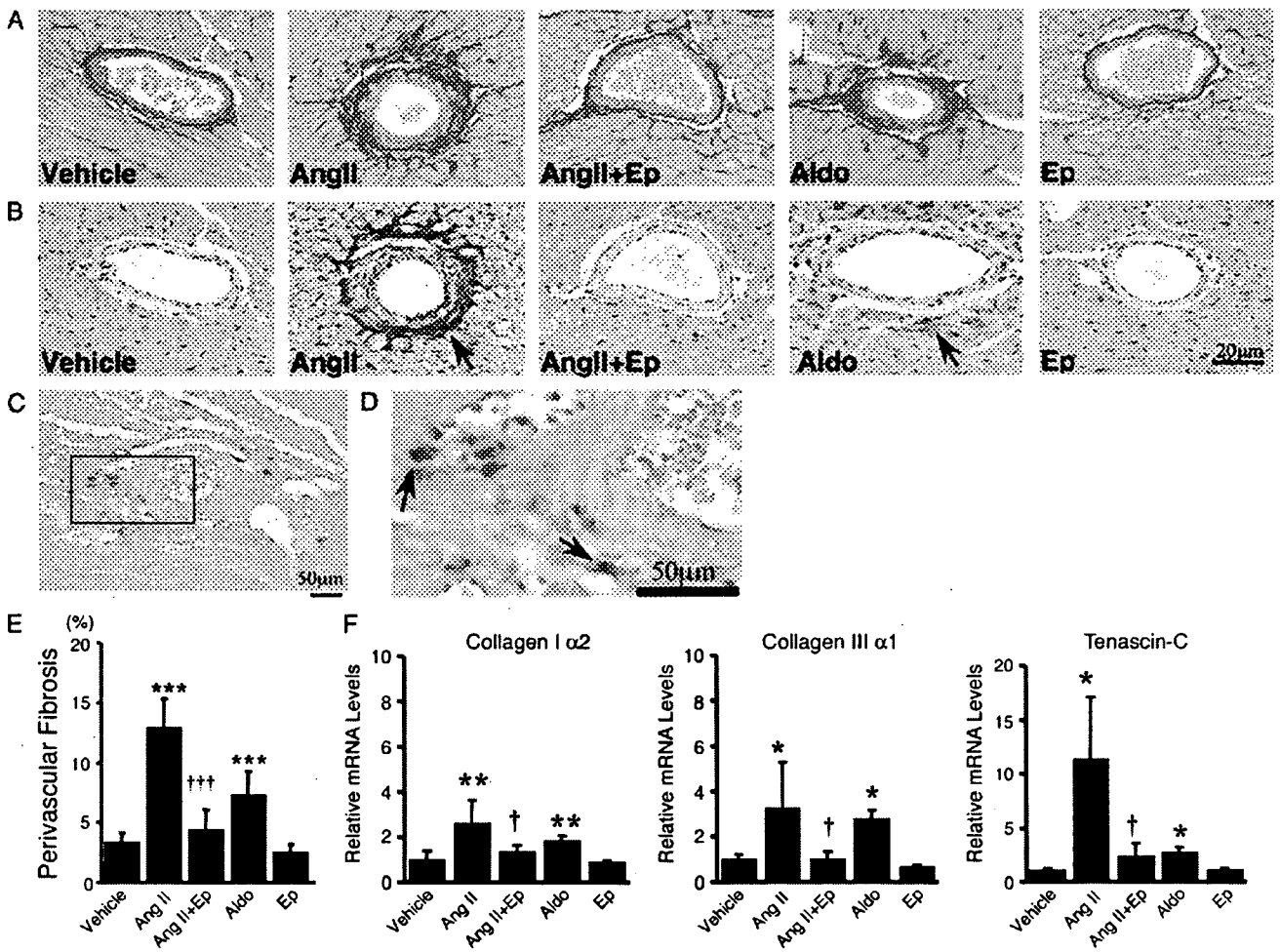

FIGURE 2. Representative photographs of perivascular areas of myocardial tissue sirius red stained (A) and immunostained for tenascin-C (B), in situ hybridization of tenascin-C mRNA in an Ang II-treated mouse (C, D). D is a high power view of the boxed areas in C. Tenascin-C becomes detectable in perivascular region (arrows in B). Interstitial fibroblasts express tenascin-C mRNA (arrows in D). Quantification of collagen volume in perivascular areas (E), and relative mRNA level of collagen type Iα2, IIIα1 and tenascin-C in myocardium (F). Values are means ± SD. Vehicle, vehicle control mice (n = 8); Ang II, Angiotensin II-treated mice (n = 6); Ang II + Ep, Ang II/eplerenone-treated mice (n = 8); Ep, eplerenone-treated mice (n = 5); Aldo, aldosterone-treated mice (n = 4). *$P < 0.05$, **$P < 0.01$, ***$P < 0.001$ vs vehicle control group. †$P < 0.05$, †††$P < 0.001$ vs Ang II-treated group.

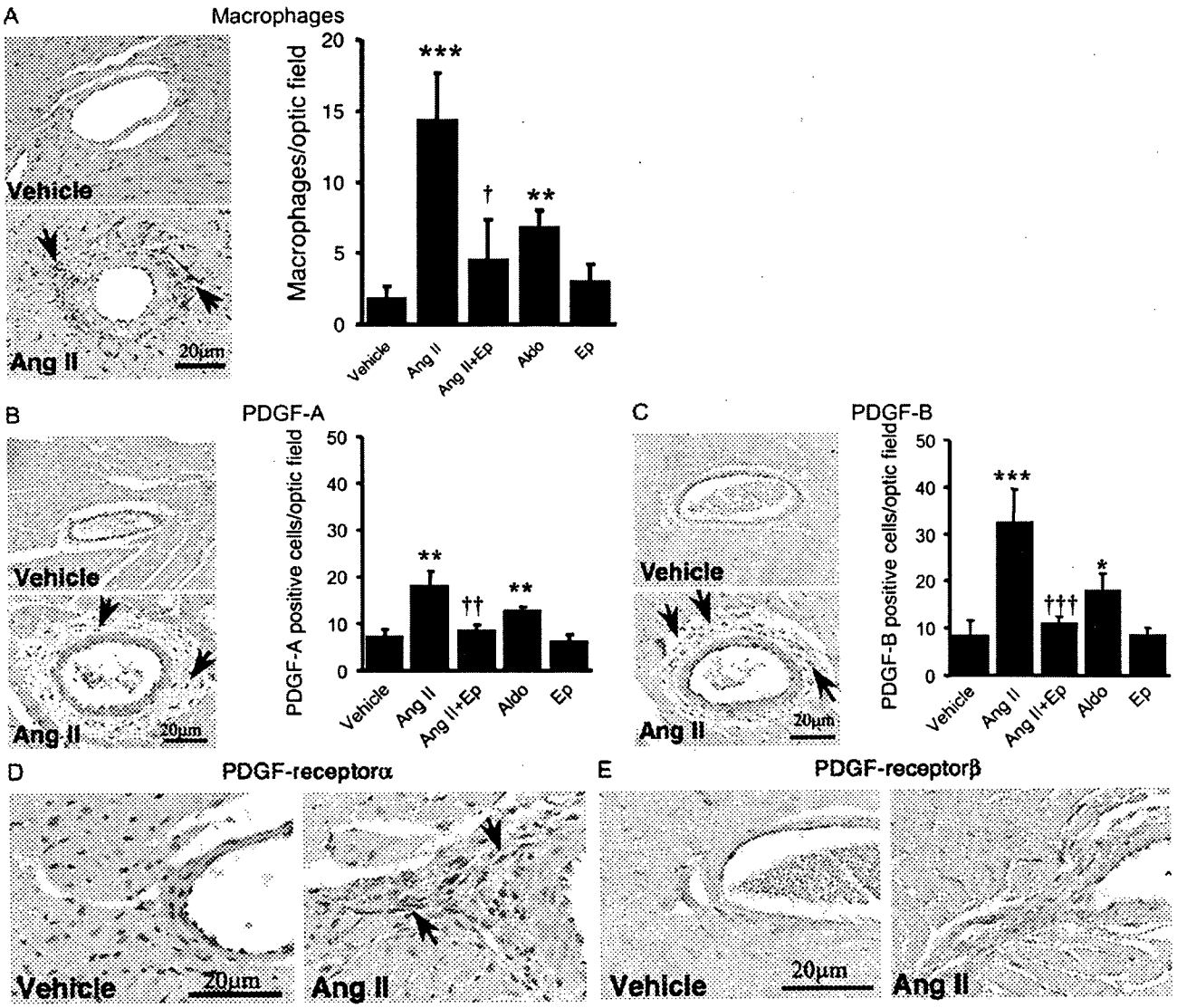

FIGURE 3. Immunohistochemial analysis of mouse myocardial tissue. Representative photographs of immunostained myocardium and numbers of positively stained cells at perivascular region in each group for Mac 3 (A), PDGF-A (B), PDGF-B (C), PDGF receptor α (D), and PDGF receptor β (E). Many macrophages, PDGF-A, and -B positive cells are seen at perivascular region of Ang II-treated mouse (arrows in A, B, and C).

field, $P < 0.01$, 17.7 ± 3.86 vs 8.23 ± 3.35 cells/optic field, $P < 0.001$, respectively). In Ang II/eplerenone-treated mice, the numbers of PDGF-A and PDGF-B positive cells were significantly reduced (8.39 ± 1.46 cells/optic field, $P < 0.01$, 10.7 ± 1.63 cells/optic field, $P < 0.001$, respectively) as compared with the Ang II-alone case. Perivascular fibroblasts in Ang II- or aldosterone-treated mouse heart upregulated the expression of PDGF receptor α (Fig. 3D) but did not express PDGF receptor β (Fig. 3E). No expression of either receptor was detected in the control group.

Real-time RT-PCR analysis (Fig. 4) showed that Ang II and aldosterone treatment significantly upregulated the mRNA levels for TGF-β1 (1.74 ± 0.20-fold, $P < 0.05$ and 1.49 ± 0.18-fold, $P < 0.05$, respectively; Fig. 4A) in the mouse myocardium when compared with the control mice (1.0 ± 0.35-fold). Eplerenone treatment significantly reduced TGF-β1 gene upregulation induced by Ang II treatment (0.67 ± 0.11-fold, $P < 0.05$). In contrast, no significant change of mRNA level of IL-1β, another major inflammatory mediator from macrophages, was observed in any of the groups (Fig. 4B).

Effects of Ang II, Aldosterone, and Inflammatory/Fibrotic Cytokines on Tenascin-C Synthesis by Cardiac Fibroblasts in Culture

The direct effects of Ang II and aldosterone on tenascin-C gene expression of cardiac fibroblasts were examined in culture by quantitative real-time RT-PCR (Fig. 5). Ang II (0 to 10^{-5} mol/L) significantly increased tenascin-C mRNA levels

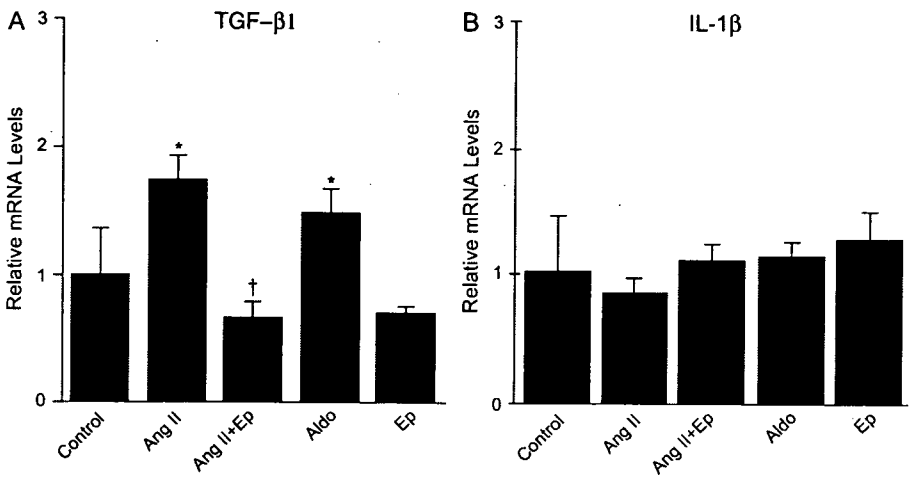

FIGURE 4. Quantitative RT-PCR analysis of proinflammatory/profibrotic mediators in mouse myocardium. Expression of TGF-β1 was increased in Ang II- and aldosterone-treated mice, and eplerenone significantly reduced this upregulation. No significant change of mRNA level of IL-1β was observed in any groups. Values are means ± SD. Vehicle, vehicle control mice (n = 10); Ang II, angiotensin II-treated mice (n = 3); Ang II + Ep, Ang II/eplerenone-treated mice (n = 5); Ep, eplerenone-treated mice (n = 3); Aldo, aldosterone-treated mice (n = 3). $*P < 0.05$ vs vehicle control group, $\dagger P < 0.05$ vs Ang II-treated group.

in a dose-dependent manner, and the expression level reached a peak at the concentration of 10^{-7} mol/L (2.1 ± 0.7-fold increase, Fig. 5A). In contrast, addition of aldosterone (0 to 10^{-6} mol/L) did not significantly affect tenascin-C expression levels at any of the concentrations examined (Fig. 5B). Eplerenone did not significantly influence Ang II-induced tenascin-C expression, and no synergism was evident with Ang II (10^{-7} mol/L) in the presence of aldosterone (10^{-8} mol/L, Fig. 5C).

To identify possible mediators of upregulation of tenascin-C expression in cardiac fibroblasts, cells were treated with PDGF-BB (Fig. 5D) and TGF-β (Fig. 5E). These factors caused a significant increase of tenascin-C expression in a dose-dependent manner.

DISCUSSION

Possible Involvement of Tenascin-C in Reactive Fibrosis of the Hypertensive Heart

Tenascin-C has been proposed to promote fibrosis because its expression is upregulated in various fibrogenic processes such as liver fibrosis,[25] lung fibrosis,[12] skin wound healing,[11] and scar formation after myocarditis.[17,18] Directly supporting this possibility, we have recently reported that locally applied tenascin-C accelerates collagen fiber formation in aneurysmal cavities in a rat model[26] and that deficiency of tenascin-C significantly attenuates liver fibrosis in an immune-mediated chronic hepatitis mouse model.[13] In the present study, we demonstrated that tenascin-C is not detected in the normal myocardium but becomes markedly upregulated in perivascular fibrosing areas in the Ang II-induced hypertensive mouse heart and that the expression level parallels the extent of fibrosis. These findings suggest that tenascin-C may be involved in the progression of reactive fibrosis, and its elevated expression might be a marker for active progression of the fibrosis in the hypertensive heart.

MECHANISM OF UPREGULATION OF TENASCIN-C GENE EXPRESSION

Previous studies demonstrated that expression of tenascin-C is upregulated with vascular remodeling in pulmonary hypertension[27,28] and spontaneous hypertensive rats[29] and that mechanical stress is an important tenascin-C–inducing factor (reviewed in reference 8). In this study, we found that upregulated expression of tenascin-C in Ang II-induced hypertensive mice was blocked by an aldosterone blocker, eplerenone, without affecting the blood pressure level, which suggests that Ang II may induce tenascin-C expression in myocardium through an aldosterone-dependent pathway but independent of blood pressure. Based on our *in situ* hybridization analysis demonstrating that the source of tenascin-C was cardiac fibroblasts in the perivascular region, we speculated that aldosterone might stimulate interstitial fibroblasts to synthesize tenascin-C. However, aldosterone did not induce tenascin-C synthesis in cardiac fibroblasts in culture, although Ang II enhanced tenascin-C expression as reported for other types of cells.[29,30] Although it remains controversial whether cardiac fibroblasts express mineral corticoid receptors,[31–33] several reports have suggested synergism between Ang II and aldosterone[34,35] because of induction of Ang II receptor levels[36] or receptor binding[37] by the latter. However, neither addition of aldosterone nor blocking with eplerenone exerted any influence on tenascin-C expression induced by Ang II in the present study. Therefore, it seems likely that aldosterone facilitates tenascin-C gene expression *in vivo* not through a direct action on cardiac fibroblasts but by actions on other factors secreted by other cells.

There is a growing body of evidence that Ang II/aldosterone treatment induces inflammation and accumulation of macrophages in perivascular regions in the myocardium.[5,6] Generally, macrophages are important regulators in inflammation in various tissue and the main source of fibrogenic mediators such as IL-1, TGF-β, and PDGF (reviewed in reference 38). In the present study, Ang II infusion caused accumulation of macrophages and upregulation of PDGF-A, -B, PDGF receptor α, and TGF-β1 in mouse hearts. These changes were inhibited by eplerenone, and their extent correlated with the expression level of tenascin-C. In culture, TGF-β1 and PDGF upregulated tenascin-C expression by cardiac fibroblasts. Taken together, it seems likely that aldosterone elicits inflammatory reaction in perivascular

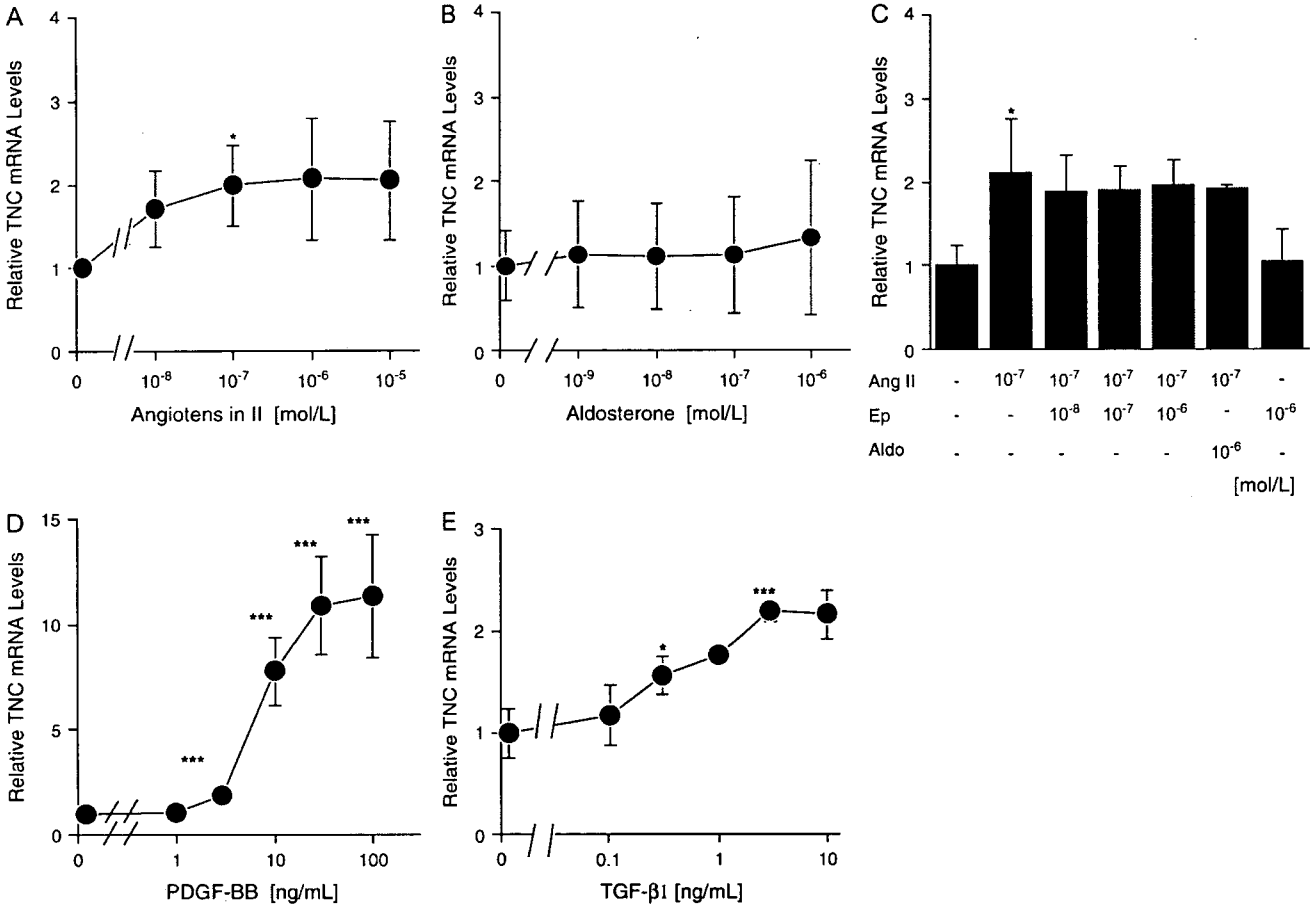

FIGURE 5. Direct effects of Ang II, aldosterone, and proinflammatory/profibrotic mediators on cultured cardiac fibroblasts. Six hours after addition of Ang II (0 to 10^{-5} mol/L) or aldosterone (0 to 10^{-6} mol/L), total RNA was extracted and relative tenascin-C mRNA levels were quantified using real-time RT-PCR. Tenascin-C mRNA levels in cardiac fibroblasts treated with Ang II were increased (A) but not with aldosterone (B). Combined effects of eplerenone (0, 10^{-8}, 10^{-7}, 10^{-6} mol/L) on Ang II (10^{-7} mol/L)-induced tenascin-C expression in cardiac fibroblasts were not observed (C). PDGF markedly upregulated the mRNA for tenascin-C (D). TGF-β1 also significantly increased tenascin-C expression. Ang II, angiotensin II-treated (E); Ep, eplerenone-treated; Aldo, aldosterone; TNC, tenascin-C; $^{*}P < 0.05$ vs no substance. Values are means ± SD. $^{*}P < 0.05$, $^{***}P < 0.001$ vs no substance.

regions in Ang II-induced hypertensive mouse hearts, which might, in turn, induce tenascin-C synthesis of fibroblasts partly through 2 signaling pathways mediated by TGFβ and PDGF-A-B/PDGF-receptor α.

Although further studies are necessary to elucidate the complex multistep molecular pathways involved, induction of tenascin-C by aldosterone in the hypertensive heart might be a key step in perivascular fibrosis and thus a prime target for therapy.

CONCLUSION

The present results suggest involvement of tenascin-C in hypertensive cardiac fibrosis and that blockade of mineralocorticoid receptor with eplerenone reduces expression of tenascin-C by reducing inflammatory reaction, subsequently resulting in attenuation of perivascular fibrosis.

ACKNOWLEDGMENTS

This study was supported by a grant-in-aid for scientific research (No. 17590725) from the Ministry of Education, Culture Sports, Science and Technology of Japan to K.I.-Y and by a grant for Intractable Disease from the Ministry of Health, Labor and Welfare of Japan to K.I.-Y and M. H. Part of the study was also supported from a grant by Pfizer, Inc.

REFERENCES

1. Silver MA, Pick R, Brilla CG, et al. Reactive and reparative fibrillar collagen remodeling in the hypertrophied rat left ventricle: Two experimental models of myocardial fibrosis. *Cardiovasc Res.* 1990;24: 741–747.
2. Weber KT, Brilla CG. Pathological hypertrophy and cardiac interstitium. Fibrosis and renin-angiotensin-aldosterone system. *Circulation.* 1991;83: 1849–1865.
3. Brilla CG, Weber KT. Reactive and reparative myocardial fibrosis in arterial hypertension in the rat. *Cardiovasc Res.* 1992;26:671–677.

4. Fiebeler A, Nussberger J, Shagdarsuren E, et al. Aldosterone synthase inhibitor ameliorates angiotensin ii-induced organ damage. *Circulation*. 2005;111:3087–3094.
5. Kuwahara F, Kai H, Tokuda K, et al. Hypertensive myocardial fibrosis and diastolic dysfunction: Another model of inflammation? *Hypertension*. 2004;43:739–745.
6. Rocha R, Rudolph AE, Frierdich GE, et al. Aldosterone induces a vascular inflammatory phenotype in the rat heart. *Am J Physiol*. 2002;283: H1802–810.
7. Endemann DH, Touyz RM, Iglarz M, et al. Eplerenone prevents salt-induced vascular remodeling and cardiac fibrosis in stroke-prone spontaneously hypertensive rats. *Hypertension*. 2004;43:1252–1257.
8. Chiquet-Ehrismann R, Chiquet M. Tenascins: Regulation and putative functions during pathological stress. *J Pathol*. 2003;200:488–499.
9. Jones FS, Jones PL. The tenascin family of ECM glycoproteins: Structure, function, and regulation during embryonic development and tissue remodeling. *Dev Dyn*. 2000;218:235–259.
10. Jones PL, Jones FS. Tenascin-c in development and disease: Gene regulation and cell function. *Matrix Biol*. 2000;19:581–596.
11. Mackie EJ, Halfter W, Liverani D. Induction of tenascin in healing wounds. *J Cell Biol*. 1988;107:2757–2767.
12. Kuhn C, Mason RJ. Immunolocalization of sparc, tenascin, and thrombospondin in pulmonary fibrosis. *Am J Pathol*. 1995;147:1759–1769.
13. El-Karef A, Yoshida T, Gabazza EC, et al. Deficiency of tenascin-c attenuates liver fibrosis in immune-mediated chronic hepatitis in mice. *J Pathol*. 2007;211:86–94.
14. Willems IE, Arends JW, Daemen MJ. Tenascin and fibronectin expression in healing human myocardial scars. *J Pathol*. 1996;179:321–325.
15. Frangogiannis NG, Shimoni S, Chang S, et al. Active interstitial remodeling: An important process in the hibernating human myocardium. *J Am Coll Cardiol*. 2002;39:1468–1474.
16. Imanaka-Yoshida K, Hiroe M, Nishikawa T, et al. Tenascin-c modulates adhesion of cardiomyocytes to extracellular matrix during tissue remodeling after myocardial infarction. *Lab Invest*. 2001;81: 1015–1024.
17. Imanaka-Yoshida K, Hiroe M, Yasutomi Y, et al. Tenascin-c is a useful marker for disease activity in myocarditis. *J Pathol*. 2002;197: 388–394.
18. Morimoto S, Imanaka-Yoshida K, Hiramitsu S, et al. The diagnostic utility of tenascin-c for evaluation of activity of human acute myocarditis. *J Pathol*. 2005;205:460–467.
19. Sato M, Toyozaki T, Odaka K, et al. Detection of experimental autoimmune myocarditis in rats by 111 in monoclonal antibody specific for tenascin-c. *Circulation*. 2002;106:1397–1402.
20. Tamaoki M, Imanaka-Yoshida K, Yokoyama K, et al. Tenascin-c regulates recruitment of myofibroblasts during tissue repair after myocardial injury. *Am J Pathol*. 2005;167:71–80.
21. Sato A, Aonuma K, Imanaka-Yoshida K, et al. Serum tenascin-c might be a novel predictor of left ventricular remodeling and prognosis after acute myocardial infarction. *J Am Coll Cardiol*. 2006;47:2319–2325.
22. Terasaki F, Okamoto H, Onishi K, et al. Higher serum tenascin-c levels reflect the severity of heart failure, left ventricular dysfunction and remodeling in patients with dilated cardiomyopathy. *Circ J*. 2007;71: 327–330.
23. Sano H, Sudo T, Yokode M, et al. Functional blockade of platelet-derived growth factor receptor-beta but not of receptor-alpha prevents vascular smooth muscle cell accumulation in fibrous cap lesions in apolipoprotein e-deficient mice. *Circulation*. 2001;103:2955–2960.
24. Sano H, Ueda Y, Takakura N, et al. Blockade of platelet-derived growth factor receptor-beta pathway induces apoptosis of vascular endothelial cells and disrupts glomerular capillary formation in neonatal mice. *Am J Pathol*. 2002;161:135–143.
25. Yamada S, Ichida T, Matsuda Y, et al. Tenascin expression in human chronic liver disease and in hepatocellular carcinoma. *Liver*. 1992;12:10–16.
26. Toma N, Imanaka-Yoshida K, Takeuchi T, et al. Tenascin-c coated on platinum coils for acceleration of organization of cavities and reduction of lumen size in a rat aneurysm model. *J Neurosurg*. 2005;103:681–686.
27. Botney MD, Kaiser LR, Cooper JD, et al. Extracellular matrix protein gene expression in atherosclerotic hypertensive pulmonary arteries. *Am J Pathol*. 1992;140:357–364.
28. Jones PL, Cowan KN, Rabinovitch M. Tenascin-c, proliferation and subendothelial fibronectin in progressive pulmonary vascular disease. *Am J Pathol*. 1997;150:1349–1360.
29. Mackie EJ, Scott-Burden T, Hahn AW, et al. Expression of tenascin by vascular smooth muscle cells. Alterations in hypertensive rats and stimulation by angiotensin ii. *Am J Pathol*. 1992;141:377–388.
30. Sharifi BG, LaFleur DW, Pirola CJ, et al. Angiotensin ii regulates tenascin gene expression in vascular smooth muscle cells. *J Biol Chem*. 1992;267: 23910–23915.
31. Lijnen P, Petrov V. Induction of cardiac fibrosis by aldosterone. *J Mol Cell Cardiol*. 2000;32:865–879.
32. Brilla CG, Zhou G, Matsubara L, et al. Collagen metabolism in cultured adult rat cardiac fibroblasts: Response to angiotensin ii and aldosterone. *J Mol Cell Cardiol*. 1994;26:809–820.
33. Neumann S, Huse K, Semrau R, et al. Aldosterone and d-glucose stimulate the proliferation of human cardiac myofibroblasts in vitro. *Hypertension*. 2002;39:756–760.
34. Hatakeyama H, Miyamori I, Fujita T, et al. Vascular aldosterone. Biosynthesis and a link to angiotensin ii-induced hypertrophy of vascular smooth muscle cells. *J Biol Chem*. 1994;269:24316–24320.
35. Mazak I, Fiebeler A, Muller DN, et al. Aldosterone potentiates angiotensin ii-induced signaling in vascular smooth muscle cells. *Circulation*. 2004;109:2792–2800.
36. Robert V, Heymes C, Silvestre J-S, et al. Angiotensin at1 receptor subtype as a cardiac target of aldosterone: Role in aldosterone-salt-induced fibrosis. *Hypertension*. 1999;33:981–986.
37. Ullian ME, Schelling JR, Linas SL. Aldosterone enhances angiotensin ii receptor binding and inositol phosphate responses. *Hypertension*. 1992; 20:67–73.
38. Martin P, Leibovich SJ. Inflammatory cells during wound repair: The good, the bad and the ugly. *Trends Cell Biol*. 2005;15:599–607.

A Novel Method of Displaying Left Ventricular Function and Dyssynchrony Using Tissue Doppler Imaging

Takahide Ito, MD, PhD; Yasunori Kawanishi, MD; Bin Tsukada, MD; Rie Futai, MD; Fumio Terasaki, MD, PhD; and Yasushi Kitaura, MD, PhD

Third Department of Internal Medicine, Osaka Medical College, Takatsuki, Japan

Running head: Display of ventricular dyssynchrony

Corresponding author: Takahide Ito, MD, Third Department of Internal Medicine, Osaka Medical College, 2-7, Daigaku-machi, Takatsuki City, Osaka, 569-8686, Japan.

FAX number: +81-726-92-8706

Telephone number: +81-726-83-1221, Ext.-2353

E-mail address: in3016@poh.osaka-med.ac.jp

Abstract

Here is proposed a simple and novel method of displaying left ventricular (LV) function and dyssynchrony using tissue Doppler imaging. We assessed clinical applicability of this method by comparing normal subjects (n = 50) and patients with left-bundle branch block (LBBB) (n = 41). The time-to-peak systolic velocities (TPVs) obtained from the 6 basal LV segments are assumed to be "vectors" and aligned radially such that each terminal point is directed to the corresponding LV segment. The constructed hexagonal graph covers the following aspects of LV function and dyssynchrony: 1) *%area-hexagon*, the percent area of the hexagon, reflecting global LV systolic function; 2) *time-delay magnitude*, the length of the composite vector for the 6 vectors; 3) *time-delay angle*, the graphical position of the composite vector, that is, the delayed contraction site. Compared with normal subjects, patients with left-bundle branch block (LBBB) had greater values of %area-hexagon and time-delay magnitude. The LBBB patients, especially those with LV systolic dysfunction (n = 23), had the time-delay angle located between the anterior and inferior segments. The new displaying method permits one-look recognition of LV function and dyssynchrony, and thus would be useful in the practice of cardiac resynchronization therapy.

Key words: dyssynchrony; tissue Doppler imaging; ventricular function.

We have developed a simple and novel method of displaying left ventricular (LV) function using tissue Doppler imaging, the most commonly used technique to assess LV dyssynchrony. This method provides the measures of global chamber function as well as systolic dyssynchrony. As with systolic dyssynchrony, the determination of the delayed contraction site and its time-delay magnitude is possible. This paper introduces the rationale of this method and its clinical applicability by comparing normal subjects with patients showing left-bundle branch block (LBBB).

Methods

Study Subjects. This study consisted of 41 patients showing an LBBB pattern on the surface electrocardiogram and 50 normal subjects. All the patients were in sinus rhythm and stable in clinical conditions, some being treated on standard cardiac medications. The normal subjects did not have evidence of cardiovascular abnormalities on routine echocardiography. Written informed consent was obtained from all the subjects to participate in this study.

Conventional Echocardiography. Standard echocardiography was performed using a commercially available apparatus (Vivid 7 echocardiographic scanner [GE-Vingmed Ultrasound, Horten, Norway]) with a 2.5-MHz transducer. The left atrial diameter was measured during systole along parasternal long-axis view from the 2-dimension guided M-mode tracing. The LV dimension and wall thickness were also calculated using M-mode method, and the LV ejection fraction was assessed by the modified Simpson's method using the apical 2 and 4-chamber views. Parameters of LV diastolic function were assessed by the pulsed Doppler method. These included LV inflow velocities of the peak early (E) and atrial filling (A) waves, their ratio (E/A), and the E wave deceleration time. Using tissue Doppler imaging, the peak wall motion velocity of the early diastolic wave (Ea) was obtained with the sample volume placed at the septal corner of the mitral annulus. The ratio of E/Ea, a surrogate for LV filling pressure, was also measured (1). The isovolumic contraction time was

determined using the timing of aortic valve opening on the LV outflow velocity profile.

Tissue Doppler imaging. The new method for displaying LV functional parameters was developed exclusively using a commercially available echocardiographic apparatus (Vivid 7, GE Vingmed, Horten, Norway). With a 4s transducer equipped with the echo-machine, we recoded color tissue Doppler images of the apical two-, four-, and long-axis chamber views. Gain settings, filters, and pulse repetition frequency were adjusted to optimize color saturation, and sector size and depth were optimized for the highest possible frame rate (>140 frames/s). At least 3 consecutive beats were digitally stored for the subsequent offline analysis. With a sample volume of 10×5 mm, we constituted regional myocardial velocity curves arising from 6 basal segments of the LV walls, namely, anteroseptal, anterior, lateral, posterior, inferior, and septal segments (Figure 1, top left). For each segment the time-to-peak systolic velocity (TPV), a time-interval between the onset of QRS complex and peak myocardial systolic velocity in ejection phase, was calculated (Figure 1, top right). To ensure that the peak was located in ejection phase, the timing of aortic opening and closure was determined by incorporating pulsed Doppler recordings of the LV outflow velocity profile. Reproducibility of TPVs was described in our previously published reports, which showed acceptable results (2).

New display of LV function and dyssynchrony. The TPVs obtained are corrected by heart rate ($\sqrt{RR}$) and assumed to be "vectors". The "vectors" are aligned radially such that they center on a common starting point and each terminal point is directed to the corresponding LV segment (Figure 1, bottom left). Then the terminal points are connected to the adjacent one, turning into a hexagon. The constructed hexagonal graph is considered to express the following aspects of LV function and dyssynchrony (Figure 1, bottom right): 1) *%area-hexagon*, the percent area of the hexagon divided by the overall graph area, reflecting global LV systolic function. The overall graph area is determined when the graph scales for each segment are all 500 ms. The rationale for

the %area-hexagon as an index of LV contractility lies in the fact that the tissue Doppler-derived TPV is correlated inversely with the first derivative of LV pressure curve (peak +dp/dt) and LV ejection fraction (3) and that the TPV superimposes the isovolumic contraction time, which is prolonged in the presence of LV dysfunction (4). Thus, the greater the %area-hexagon, the poorer LV systolic function. The shape of the hexagon also offers visual impression of LV dyssynchrony. With no-dyssynchrony, the graph shape is equilateral or symmetrical; 2) *time-delay magnitude*, the length (time [ms] in unit) of the composite vector for the 6 vectors. With no-dyssynchrony, the time-delay magnitude is 0 ms; 3) *time-delay angle*, the graphical position of the composite vector, that is, the delayed contraction site (°). If its terminal point is directed to the posterior segment ("pst" as in Figure 1), for instance, the time-delay angle is 180°. All of these parameters are calculated using the prototype custom software. The software program can also calculate 3 more measures of LV dyssynchrony: the standard deviation (SD) of TPVs; the coefficient of variance (SD divided by mean) of TPVs; and the dispersion of TPVs. Variables obtained were compared between normal subjects and LBBB patients.

Statistical analysis. All data are presented as mean±SD. A p value of <0.05 is considered significant. Continuous variables between the groups were compared by ANOVA and subsequent Sheffe's multiple comparison tests. Single linear regression analysis was used to estimate correlations between echocardiographic parameters.

Results

The LBBB patients were divided into 2 groups based on the presence or absence of LV systolic dysfunction (LV ejection fraction <50%). There were 23 patients who had LV systolic dysfunction. Table 1 shows clinical and conventional echocardiographic parameters of the resultant study groups. Among the patients with LV systolic dysfunction, 8 had significant mitral regurgitaion and 5 had

prior myocardial infarction. In the patients with preserved systolic function, there were no appreciable valvular or myocardial abnormalities causing LBBB. There were no significant differences in age and gender distribution. LV ejection fraction was depressed in the patient groups, but the difference was not statistically significant between the normal subjects and the patients with preserved systolic function. There were no significant differences with regard to the pulsed Doppler parameters of LV diastolic function, although the range of these was apparently greater in the patients with systolic dysfunction, indicating various LV diastolic abnormalities from abnormal relaxation to restrictive physiology. The tissue Doppler of the mitral annulus clearly discriminated diastolic abnormalities, with a significant depression of the Ea and E/Ea in the patients with systolic dysfunction compared with the other groups.

Table 2 summarizes the measurements of TPVs and the results of the new method. The TPVs were much greater for all the segments in the patients from LBBB groups compared with normal subjects. This finding was associated with greater %area-hexagon for the patients. In normal subjects, %area-hexagon was less than 10% with no overlap with LBBB patients who had systolic dysfunction (Figure 2). The %area-hexagon had positive correlation with isovolumic relaxation time ($r=0.80$, $p<0.0001$) and negative correlation with LV ejection fraction ($r=-0.68$, $p<0.0001$) (Figure 2). Figure 3 shows the scatter-plots of the time-delay magnitude against the time-delay angle. The LBBB patients, especially those with systolic dysfunction, had the time-delay angle located between the anterior and inferior segments (60° to 240°) with the mean time-delay magnitude around 100 ms. In the normal subjects, on the other hand, the time-delay angle was evenly distributed all over the segments with the time-delay magnitude mostly less than 100 ms. The incidence of the time-delay angle being located in the LV free wall was 87% in the patients with systolic dysfunction compared with 46% in the normal subjects ($p<0.01$). Representative analyses of the new method are shown in Figure 4.

Discussion

We have proposed a new method for displaying LV function and dyssynchrony using tissue Doppler imaging. This method provides 3 major parameters related to LV dyssynchrony and function: 1) %area hexagon; 2) time-delay magnitude; and 3) time-delay angle. The measurements of these parameters were obviously altered in LBBB patients when compared with normal subjects. This method would be applied in the practice of cardiac resynchronization therapy.

The %area-hexagon, a percent area of the hexagon made by connecting terminal points of the 6 vectors, is considered to be an indexed TPV. Yamada et al demonstrated clinical usefulness of tissue Doppler-derived parameters for the evaluation of LV systolic function (3). They observed that the time from the electrocardiographic Q-wave to the peak systolic myocardial velocity, as the TPV in the present study, was correlated with the peak +dp/dt as well as LV ejection fraction. The TPV was shown to be prolonged in various disease conditions (3,4) and the %area-hexagon is roughly a sum of the six TPVs. Thus, the greater value indicates the poorer LV systolic function. In our finding, there was no overlap of the %area-hexagon between the normal subjects and patients with LBBB and LV systolic dysfunction.

A number of echocardiographic techniques/parameters for the assessment of LV dyssynchrony have been proposed. M-mode recordings of septal-to-posterior wall motion delay (5) and the analysis of a single imaging plane (e.g., 4-chamber view) (6) are simple methods for assessing LV dyssynchrony; however, any dyssynchrony in other walls can be overlooked. Three-dimensional technique appears to overcome this limitation (7), although the relatively lower spatial resolution may restrict its clinical feasibility. On the other hand, tissue Doppler-derived long-axis function is most commonly used to confirm LV dyssynchrony and select potential responders of cardiac resynchronization therapy. Yu et al reported that SD of TPVs in ejection phase among the 12 basal

and middle myocardial segments was not only the strongest indicator of LV dyssynchrony but also the most powerful predictor of the clinical outcome after cardiac resynchronization therapy (8,9). The receiver operating characteristics curve for predicting LV reverse remodeling demonstrated an area under the curve of 0.90 with 12-segmental analysis compared to 0.70 with 6-basal segmental analysis (9). We currently employed 6-segmental analysis, which appears to be inferior. However, other investigators who examined 2- to 6-basal segments found that the parameters derived were useful for predicting reverse remodeling (6,10). Moreover, it is tempting to be speculated that the LV pacing lead should be positioned near the basal segments since the basal part of the LV wall is activated last in LBBB patients (11). The priority of the new method lies in how more easily parameters can be obtained and how more detail information can be available from individual subjects. The new method permits simultaneous and one-look recognition of the delayed contraction site, its time-delay as well as global LV function.

In the current observation, the patients with LV systolic dysfunction had the time-delay angle located between the anterior and inferior segments (60° to 240°). This finding is consistent with a previous study using tissue Doppler imaging, in which the latest mechanical activity was frequently located in the lateral wall followed by the anterior and posterior regions (12). Some of the normal subjects had an increased time-delay, indicating that dyssynchrony is not a specific finding in heart disease patients. Thus, global LV function should be taken into consideration when assessing dyssynchrony in individual subjects. We also observed the strong correlation between %area-hexagon and isovolumic contraction time. The isovolumic contraction time was shown to be shortened after successful cardiac resynchronization therapy (12). The new method, when applied in subjects receiving successful procedure, would reveal decreases in %area-hexagon and time-delay magnitude. Further study is necessary to prove the practical use of the new method on cardiac resynchronization therapy.

References

1. Nagueh SF, Middleton KJ, Kopelen HA, Quinones MA. Doppler tissue imaging: a noninvasive technique for evaluation of left ventricular relaxation and estimation of filling pressures. *J Am Coll Cardiol.* 1997;30:1527–1533.
2. Ito T, Suwa M, Sakai Y, Hozumi T, Kitaura Y. Usefulness of tissue Doppler imaging for demonstrating altered septal contraction sequence during dual-chamber pacing in obstructive hypertrophic cardiomyopathy. *Am J Cardiol* 2005;96:1558-1562.
3. Yamada H, Oki T, Tabata T, Iuchi A, Ito S. Assessment of left ventricular systolic wall motion velocity with pulsed tissue Doppler imaging: comparison with peak dp/dt of the left ventricular pressure curve. *J Am Soc Echocardiogr* 1998;11:442-449.
4. Tei C, Ling LH, Hodge DO, Bailey KR, Oh JK, Rodeheffer RJ, Tajik AJ, Seward JB. New index of combined systolic and diastolic myocardial performance: a simple and reproducible measure of cardiac function: a study in normals and dilated cardiomyopathy. *J Cardiol* 1995;26:357-366.
5. Pitzalis MV, Iacoviello M, Romito R, Massari F, Rizzon B, Luzzi G, Guida P, Andriani A, Mastropasqua F, Rizzon P. Cardiac resynchronization therapy tailored by echocardiographic evaluation of ventricular asynchrony. *J Am Coll Cardiol* 2002;40:1615-1622.
6. Bax JJ, Bleeker GB, Marwick TH, Molhoek SG, Boersma E, Steendijk P, van der Wall EE, Schalij MJ. Left ventricular dyssynchrony predicts response and prognosis after cardiac resynchronization therapy. *J Am Coll Cardiol* 2004;44:1834-1840.
7. Zhang Q, Yu CM, Fung JW, Zhang Y, Chan YS, Chan HC, Yip GW, Sanderson JE. Assessment of the effect of cardiac resynchronization therapy on intraventricular mechanical synchronicity by regional volumetric changes. *Am J Cardiol* 2005;95:126-129.
8. Yu CM, Chau E, Sanderson JE, Fan K, Tang MO, Fung WH, Lin H, Kong SL, Lam YM, Hill

MR, Lau CP. Tissue Doppler echocardiographic evidence of reverse remodeling and improved synchronicity by simultaneously delaying regional contraction after biventricular pacing therapy in heart failure. *Circulation* 2002;105:438-445.

9. Yu CM, Zhang Q, Fung JW, Chan HC, Chan YS, Yip GW, Kong SL, Lin H, Zhang Y, Sanderson JE. A novel tool to assess systolic asynchrony and identify responders of cardiac resynchronization therapy by tissue synchronization imaging. *J Am Coll Cardiol* 2005;45:677-684.
10. Notabartolo D, Merlino JD, Smith AL, DeLurgio DB, Vera FV, Easley KA, Martin RP, León AR. Usefulness of the peak velocity difference by tissue Doppler imaging technique as an effective predictor of response to cardiac resynchronization therapy. *Am J Cardiol* 2004;94:817-820.
11. Auricchio A, Fantoni C, Regoli F, Carbucicchio C, Goette A, Geller C, Kloss M, Klein H. Characterization of left ventricular activation in patients with heart failure and left bundle-branch block. *Circulation* 2004;109:1133-1139.
12. Ansalone G, Giannantoni P, Ricci R, Trambaiolo P, Fedele F, Santini M. Doppler myocardial imaging to evaluate the effectiveness of pacing sites in patients receiving biventricular pacing. *J Am Coll Cardiol* 2002;39:489-499.

Figure Legends

Figure 1.

Top left, a schema of apical 2-. 4- and long-axis views where segments to be analyzed are depicted; Top right, a representative myocardial velocity curve arising from the basal septum; Bottom left, the "vectors" of the 6 TPVs, each corrected by heart rate (TPVc), being arranged radially; Bottom right, a completed display of LV function and dyssynchrony. AVC, aortic valve closure; AVO, aortic valve opening; ant, anterior wall; asp, anteroseptal wall; inf, inferior wall; lat, lateral wall; pst, posterior wall; sp, septum.

Figure 2.

Correlations of the %area-hexagon with isovolumic contraction time (left) and LV ejection fraction (right). Open circles indicate normal subjects, closed circles LBBB patients with LVEF ≥50%, and closed squares LBBB patients with LVEF <50%.

Figure 3.

Scatter-plots showing the relationship between the time-delay magnitude and time-delay angle. Other abbreviations are the same as in Figure 1. Markers are the same as in Figure 2.

Figure 4.

Top, Representative analyses of tissue Doppler imaging from a patient with LBBB and LV dysfunction (right) and form a normal subject (left); Bottom, The displays by the new method for the corresponding subjects in the top. The maximal graph scales are magnified to 350 ms. Abbreviations are the same as in Figure 1.

Table 1. Clinical and conventional echocardiographic parameters in LBBB patients and normal subjects.

	LBBB LVEF<50% (n = 23)	LBBB LVEF>50% (n = 18)	Normal (n = 50)	p Value
Age	67±11	66±9	61±14	0.114
Female (n)	6	5	26	0.277
Prior myocardial infarction	8	0	-	0.019
Significant mitral regurgitaion	5	0	-	0.058
Heart rate	70±9	67±8	68±9	0.602
QRS width	150±40*	155±35*	68±15	<0.001
Left atrial diameter (mm)	43±5*	41±7*	32±4	<0.001
LV end-diastolic dimension (mm)	65±8*†	52±8	48±5	<0.001
LV end-systolic dimension (mm)	52±11*†	32±8	30±4	<0.001
IVS (mm)	8±2*	8±1*	7±1	<0.001
PW (mm)	8±2*	8±1*	7±1	<0.001
LV end-diastolic volume (ml)	123±55*†	66±25	59±12	<0.001
LV end-systolic volume (ml)	86±47*†	29±13	23±6	<0.001
LVEF (%)	31±12*†	57±5	62±6	<0.001
E (cm/s)	62±27	63±19	68±16	0.420
A (cm/s)	62±26	69±22	70±19	0.355
E/A	1.44±1.53	1.08±0.67	1.05±0.42	0.206

E-wave deceleration time (ms)	204±74	203±56	197±52	0.864
Ea (cm/s)	5.3±1.6*†	7.3±1.0*	9.6±2.6	<0.001
E/Ea	13.1±7.9*†	8.7±2.5	7.5±2.2	<0.001
Isovolumic contraction time (ms)	144±50*	116±30*	67±14	<0.001

*p<0.01 vs. normal subjects; †p<0.01 vs. LBBB patients with LVEF>50%. IVS, thickness of the ventricular septum; LVEF, left ventricular ejection fraction; PW, thickness of the posterior wall.

Table 2. Tissue Doppler-derived parameters in LBBB patients and normal subjects.

	LBBB LVEF<50% (n = 23)	LBBB LVEF>50% (n = 18)	Normal (n = 50)	p Value
TPVs of the 6 segments (ms)				
Anteroseptal wall	189±49*	185±34*	127±24	<0.001
Anterior wall	220±74*†	176±21*	125±20	<0.001
Lateral wall	239±81*	219±66*	143±34	<0.001
Posterior wall	230±68*	233±56*	134±27	<0.001
Inferior wall	233±69*	216±40*	134±27	<0.001
Septum	210±51*	189±27*	130±23	<0.001
Variables of the new displaying method				
%Area-hexagon (%)	20.7±10.8*	17.3±5.5*	7.1±1.6	<0.001
Time-delay magnitude (ms)	115±59*	110±61*	52±42	<0.001
Time-delay angle (°)	181±67	196±85	176±100	-
SD-6	42±17*	38±16*	21±14	<0.001
CV-6	0.18±0.08	0.17±0.05	0.16±0.12	0.532
Dispersion of TPVs (ms)	111±42*	98±38*	56±38	<0.001

*p<0.01 vs. normal subjects; †p<0.01 vs. LBBB patients with LVEF>50%. CV, coefficient of variance; LVEF, left ventricular ejection fraction; SD, standard deviation; TPV, time-to-peak systolic velocity.

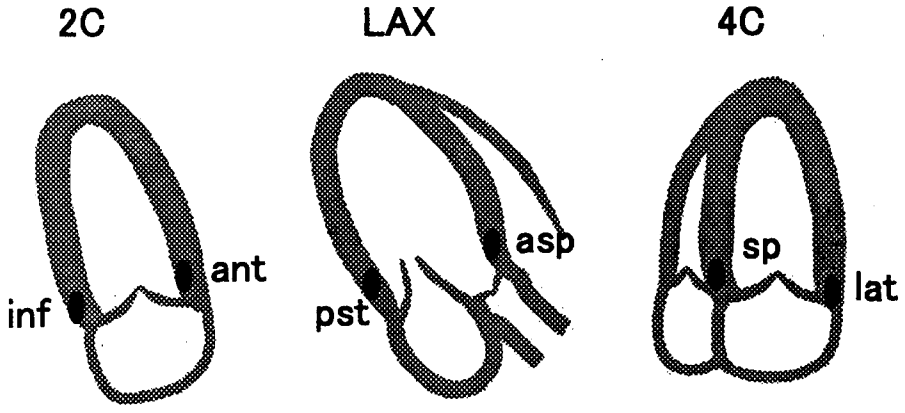
2C
LAX
4C
ant
inf
asp
pst
sp
lat

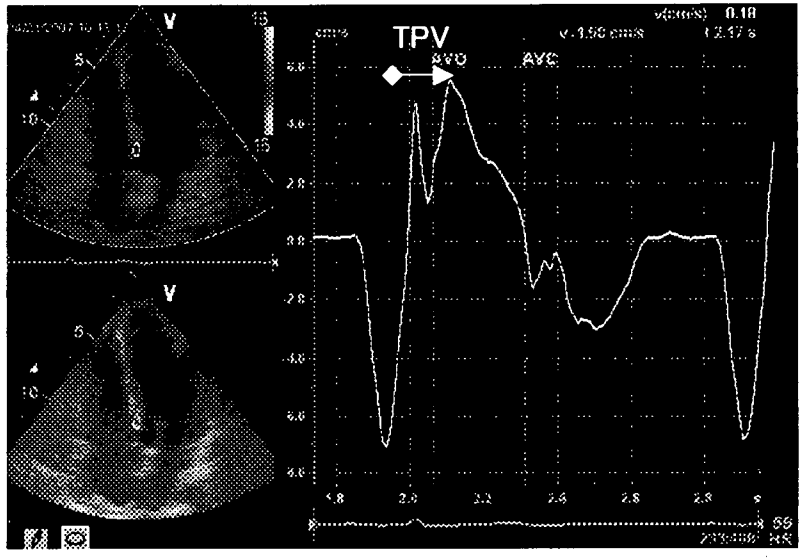
TPV

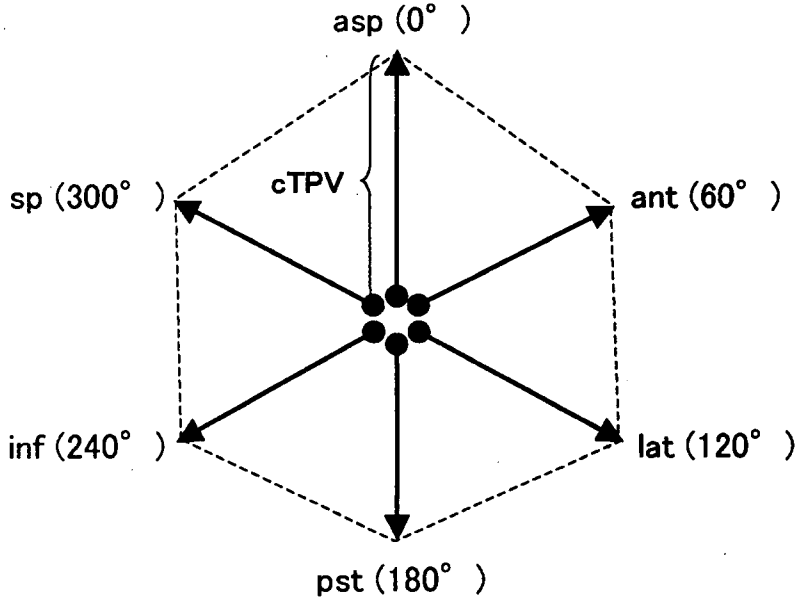
asp (0°)
cTPV
sp (300°)
ant (60°)
inf (240°)
lat (120°)
pst (180°)

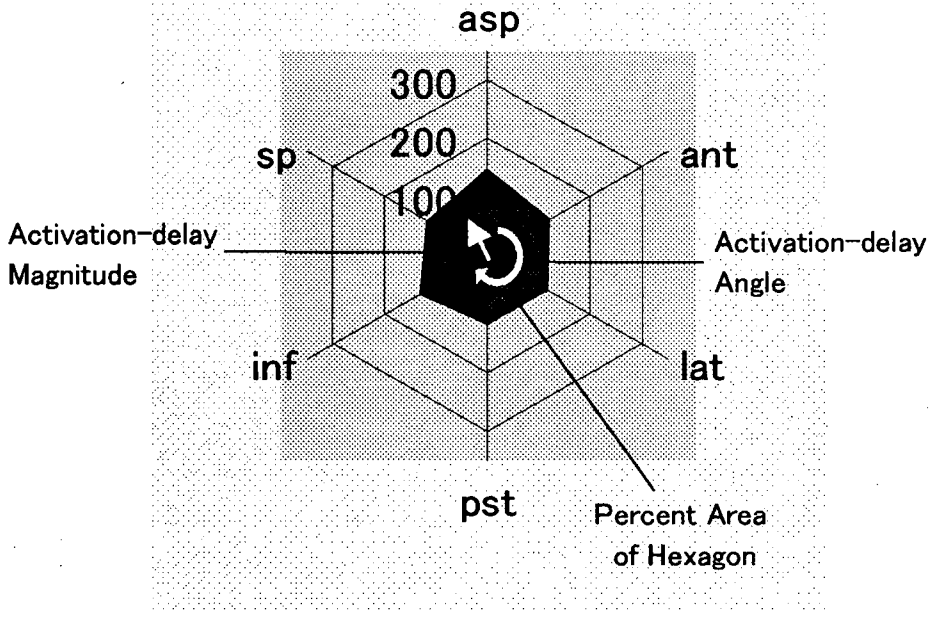
asp
300
200
100
sp
ant
Activation-delay
Magnitude
Activation-delay
Angle
inf
lat
pst
Percent Area
of Hexagon

Figure 1